Effective interactions and nuclear structure using 180 MeV protons. III. $^{30}Si(p,p')$

J. J. Kelly,[a] Q. Chen,[b] P. P. Singh,[b] M. C. Radhakrishna,[b] W. P. Jones,[b] and H. Nann[b]
[a]*Department of Physics, University of Maryland, College Park, Maryland 20742*
[b]*Department of Physics, Indiana University, Bloomington, Indiana 47401*
(Received 27 November 1989)

Differential cross sections and analyzing powers for low-lying states of ^{30}Si have been measured using 180 MeV protons. The data were analyzed using an empirical effective interaction previously fitted to inelastic scattering data for ^{16}O and ^{28}Si at the same energy. Proton transition densities for the 2_1^+, 2_2^+, 3_1^-, and 4_2^+ states were fitted to the available electron scattering data. Neutron transition densities for these states were then extracted from the proton scattering data. The fitted matrix elements M_n/M_p agree well with lifetime data for the $A=30$ $T=1$ multiplet. Results for the positive-parity states are also compared with shell-model calculations. We find that neutron densities for the 2_2^+ and 4_2^+ states are considerably stronger than predicted. We also find $M_n/M_p=1.3\pm0.1$ for the 3_1^- state and that the neutron form factor is consistent with a dominant $2s_{1/2}\rightarrow 1f_{7/2}$ transition.

I. INTRODUCTION

Traditionally, high-precision transition charge densities obtained from electron scattering measurements have provided some of the most detailed and quantitative tests of nuclear structure theories.[1,2] Recently, the shell model has achieved considerable success in describing transition densities for positive parity states in the *sd* shell.[3] Yet, comparable tests of neutron transition densities are largely unavailable. For the most part, we rely upon isospin symmetry to extract neutron matrix elements from lifetime data[4] or upon strongly absorbed probes to determine ratios between neutron and proton transition strengths.[5,6] In either case, only a single moment dominated by small densities at large radii is obtained. However, it has recently been shown that proton scattering data is capable, in principle, of yielding neutron transition densities with good radial sensitivity provided that the effective interaction is known.[7,8]

In this paper, the third in a series of three papers discussing proton scattering data at 180 MeV,[9,10] we employ an empirical effective interaction to extract neutron transition densities for several states of ^{30}Si for comparison with lifetime data and shell-model predictions. The experiment is described in Sec. II. Section III reviews the methods used to fit transition densities to scattering data and outlines the shell-model description of these densities. Results for both proton and neutron transition densities for the 2_1^+, 2_2^+, 3_1^-, and 4_2^+ are presented in Secs. IV A and IV B. Detailed comparisons are made in Sec. IV C between data for the positive-parity states and models of core polarization. The implications of uncertainties in the reaction mechanism are discussed in Sec. IV D. Finally, our conclusions are summarized in Sec. V.

II. EXPERIMENT

The experiment was performed using 180 MeV polarized protons at the Indiana University Cyclotron Facility. The experiment has previously been described in the preceding papers.[9,10] Further details may be found in Ref. 11. The ^{30}Si target was made by depositing 11.2 mg/cm^2 isotopically enriched silicon (95.5% ^{30}Si) on a carbon film. The uncertainty in target thickness is estimated to be about $\pm 10\%$.

Measurements were made for center-of-mass angles between about 6° and 74° in steps of 2°–3°. A sample spectrum is shown in Fig. 1. Data were obtained for the ground state, the 2_1^+ state at 2.235 MeV, the 2_2^+ state at 3.499 MeV, the 3_1^- state at 5.488 MeV, the 4_1^+ state at 5.279 MeV, and the 4_2^+ state at 5.950 MeV. We assume that the contribution of the 3_2^+ state at 5.231 MeV, which could not be separated from the 4_1^+ peak, is negligible. The fact that the 4_1^+ analyzing power displays the strong oscillatory pattern characteristic of normal-parity excitations by 180 MeV protons supports this assumption. Although the 0_3^+ state at 5.372 MeV was included in the analysis, its position between the stronger 4_1^+ and 3_1^- peaks obviated reliable extraction. Finally, 2_3^+ and 3_1^+ states at 4.809 and 4.831 MeV could not be resolved and are reported as a doublet.

Elastic scattering data for ^{30}Si are compared in Fig. 2 with our data[10] for ^{28}Si and those of Schwandt *et al.*[12] The enhanced structure in the ^{30}Si cross section for large momentum transfer reveals the effect of $2s_{1/2}$ neutrons, whereas the two analyzing power angular distributions are quite similar. The data for the 2_1^+, 2_2^+, 3_1^-, 4_1^+, and 4_2^+ states will be presented in Sec. IV B. Data tables are on deposit with the Physics Auxiliary Publication Service (PAPS).[13]

III. TRANSITION DENSITIES

A. Definitions and fitting procedures

The states of interest are reached by normal-parity transitions [$\Delta\pi=(-)^{\Delta J}$] driven primarily by matter den-

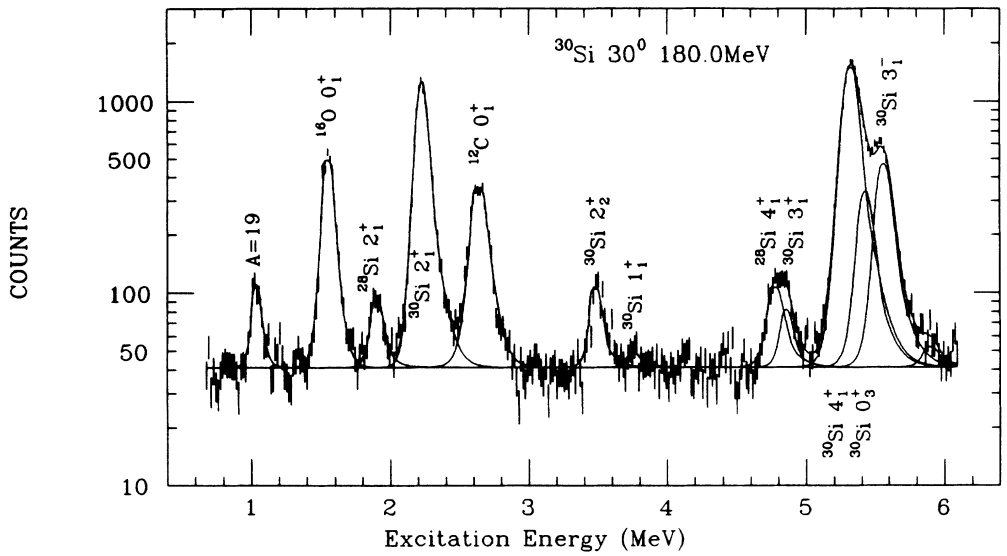

FIG. 1. Inelastic portion of a fitted spectrum for the scattering of 180 MeV protons through 30° by a ^{30}Si target.

sities of the form

$$\rho_{J\tau}(r)=\sum_i \left\langle f \left| \left| \frac{\delta(r-r_i)}{r^2} Y_J(\hat{r}_i) \right| \right| i \right\rangle , \tag{1}$$

where the sum runs over either protons or neutrons when $\tau=p$ or n, respectively. The strength of the transition can be described by the multipole moment $M_{J\tau}$ and the shape of the transition density by the transition radius $R_{J\tau}$ where

$$M_{J\tau}=\int dr\, r^{J+2}\rho_{J\tau}(r) , \tag{2a}$$

$$R^2_{J\tau}=\int dr\, r^{J+4}\rho_{J\tau}(r)/M_{J\tau} . \tag{2b}$$

Henceforth, the subscript J will be omitted for brevity whenever possible.

It is useful to define proton and neutron form factors by

$$F_\tau(q)=\frac{\sqrt{4\pi}}{N_\tau}\int dr\, r^2 j_J(qr)\rho_\tau(r) = \frac{\sqrt{4\pi}}{N_\tau}\tilde{\rho}_\tau(q) , \tag{3}$$

where $N_p=Z$ and $N_n=N$ are the numbers of protons and neutrons, respectively. Note that our normalization gives $F_n=F_p$ for the hydrodynamic model $\rho_n=(N/Z)\rho_p$. The charge form factor observed in electron scattering is now

$$F_{\rm ch}(q)=\frac{\sqrt{4\pi}}{Z}\tilde{\rho}_{\rm ch}(q) , \tag{4a}$$

$$\tilde{\rho}_{\rm ch}(q)=\tilde{\rho}_p(q)\tilde{f}_p(q)+\tilde{\rho}_n(q)\tilde{f}_n(q) , \tag{4b}$$

where $\tilde{f}_p$ and $\tilde{f}_n$ are proton and neutron charge form factors.[14]

It is convenient to express a transition density $\rho_J(r)$ as a Laguerre-Gaussian expansion (LGE) of the form[7]

$$\rho_J(r)=x^J e^{-x^2}\sum_n C_n L_n^{J+1/2}(2x^2) , \tag{5}$$

where b is an oscillator parameter and where $x=r/b$. Although the expansion is complete for any value of b, we expect the representation to be simplest, i.e., have the smallest number of significant terms, if b is chosen according to the shell model. Hence, we choose $b=1.835$ fm for ^{30}Si.[3] For the charge density, we obtain an initial

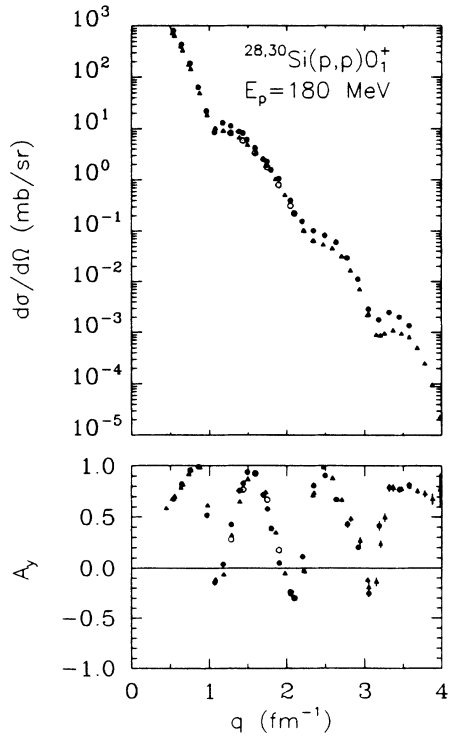

FIG. 2. Comparison between elastic scattering data for ^{30}Si (solid circles) and for ^{28}Si (open circles are from Ref. 10 and triangles are from Ref. 12).

estimate of the coefficients C_n by performing a plane-wave fit to electron scattering data. Good fits are obtained using only 2 or 3 parameters.

The coefficients with $n > 2$ can then be used to estimate the incompleteness error associated with the limited range of momentum transfer.[15] This estimate, using the methods described in Refs. 7 and 15, was made by adding pseudodata beyond a maximum momentum transfer q_m in steps of 0.2 fm^{-1} subject to the high-q bias

$$\rho_J(q) < \rho_J(q_m)(q_m/q)^4 . \tag{6}$$

We chose $q_m = 2.7$ fm^{-1} corresponding to about twice the Fermi momentum, beyond which form factors are expected to decrease rapidly with q.

We also apply a large-r or tail bias to the fitted density in order to damp the unreasonable oscillations that tend to result when high quality data are not available at small momentum transfer. This bias is enforced by adding to the chi-square function a penalty function

$$\chi_t^2 = \sum w_i[t(r_i) - \rho(r_i)]^2 , \tag{7}$$

which inhibits deviations of the fitted density $\rho(r)$ from a radial tail of the form

$$t(r) = \frac{se^{-dr}}{r^2} \tag{8}$$

beyond a match radius r_m. The parameters s and d are matched to the fit at r_m. The weights were chosen as $w_i = [wt(r_i)]^{-2}$, with $w = 1$. For charge densities, the penalty function included $N_t = 15$ points beyond $r_m = 5.0$ fm in steps of 0.2 fm. For neutron densities, which have a somewhat smaller radial extent, we chose $r_m = 4.5$ fm and $N_t = 17$. With these choices, the oscillations are damped at the expanse of only about 10% in χ^2.

1. Electron scattering

The initial analysis of electron scattering data was performed in plane-wave approximation using only a few terms of the LGE. These results were then used to supply initial parameters to a modified version of the distorted-wave code HADES.[16] Although distortion corrections are small, the more sophisticated analysis is required to obtain realistic estimates of the error envelopes describing uncertainties in the fitted density. Hence, although our fitted densities for the 2^+ states agree well with Miskimen *et al.*,[17] our error estimates are more realistic. The incompleteness error, neglected by Miskimen *et al.*, dominates the error bands because the experimental range for q is so small.

2. Proton Scattering

The analysis of proton scattering data was performed using the code LEA,[18] standing for linear expansion analysis, and methods previously described in Refs. 7 and 8. Proton densities were obtained by unfolding the nucleon form factor from the fitted charge densities and were held fixed during the analysis. The dominant interaction components are the isoscalar spin-independent central and isoscalar spin-orbit contributions. For these we used the density-dependent empirical effective interaction that was previously fitted to 180 MeV proton inelastic scattering data for six states of ^{16}O and five states of ^{28}Si simultaneously.[10] That interaction gives a better description of inelastic scattering data for normal-parity isoscalar transitions than does any available theoretical interaction and hence should yield more accurate structure results. For the isovector interaction, which makes only a small contribution to the cross section, we used the Paris-Hamburg (PH) G matrix.[19] Distortion was provided by microscopic optical potentials produced by folding these same interactions with the ground-state density, assuming that ρ_n is proportional to the ρ_p obtained from electron scattering.[20] The density-dependence of the transition potentials was enhanced by the rearrangement factor $(1+\rho\,\partial/\partial\rho)$.[21,22]

Additional uncertainties of $\pm 5\%$ in cross section and ± 0.05 in A_y were folded into the experimental data to compensate, in part, for residual uncertainties in the effective interaction. These uncertainties affect weights assigned to data points but are omitted from plots. In addition, a global uncertainty of $\pm 10\%$ in cross section normalization was assumed. Uncertainties in the fitted neutron density due to uncertainties in normalization were estimated by comparing fits made to renormalized cross-section data. The final error bands include statistical uncertainties in the data, the effects of penetrability and distortion, incompleteness errors due to limitation of momentum transfer, and uncertainties due to normalization. The incompleteness error tends to dominate $\delta\rho(r)$ for $r \lesssim 1$ fm, whereas normalization uncertainty tends to dominate for $r \gtrsim 1$ fm.

3. Parameter uncertainties

Fitted parameters are listed in Table I for transition charge densities and in Table II for neutron transition densities. For each state, the first two or three terms of the Laguerre-Gaussian expansion (LGE) suffice to describe the density with good accuracy. Higher coefficients are used to enforce high-q and large-r constraints and to provide realistic estimates of the uncertainty in the fitted density. Parameter uncertainties were estimated from the diagonal elements of the error matrix. These diagonal elements are sufficient to generate an approximation to the error band based upon the full error matrix that is fairly accurate for $r < r_m$. However, the tail bias introduces correlations which reduce $\delta\rho$ for $r > r_m$ and consequently reduces the estimated uncertainties in the moments $M_{J\tau}$ and $R_{J\tau}$.

B. Shell-model densities

Brown, Radhi, and Wildenthal[3] have surveyed 2^+ and 4^+ form factors throughout the *sd* shell. In their model, transition densities are divided into valence (v) and core (c) contributions

$$\rho_\tau(r) = \rho_\tau^v(r) + \rho_\tau^c(r) . \tag{9}$$

The valence configurations were computed in the ($1d_{5/2}$,

TABLE I. Transition charge density parameters for ^{30}Si. LGE coefficients C_n are in units of e fm^{-3} and are based upon $b=1.835$ fm. The units of M_p are e fm^J and the units of R_{ch} are fm.

	2_1^+	2_2^+	3_1^-	4_2^+
C_0	$(4.164\pm0.091)\times10^{-2}$	$(2.989\pm0.11)\times10^{-2}$	$(2.753\pm0.078)\times10^{-2}$	$(1.400\pm0.029)\times10^{-2}$
C_1	$(-2.965\pm0.053)\times10^{-2}$	$(-1.331\pm0.054)\times10^{-2}$	$(-7.970\pm0.43)\times10^{-3}$	$(-1.761\pm0.15)\times10^{-3}$
C_2	$(5.082\pm0.52)\times10^{-3}$	$(1.110\pm0.42)\times10^{-3}$	$(1.897\pm0.15)\times10^{-3}$	$(4.862\pm4.9)\times10^{-5}$
C_3	$(3.479\pm2.0)\times10^{-4}$	$(4.107\pm1.4)\times10^{-4}$	$(-4.012\pm1.3)\times10^{-4}$	$(1.465\pm2.4)\times10^{-5}$
C_4	$(-1.724\pm1.4)\times10^{-4}$	$(-1.543\pm8.2)\times10^{-5}$	$(1.113\pm0.52)\times10^{-4}$	$(1.233\pm0.67)\times10^{-5}$
C_5	$(-9.757\pm6.4)\times10^{-5}$	$(-5.342\pm2.9)\times10^{-5}$	$(-5.037\pm2.6)\times10^{-5}$	$(-7.878\pm4.4)\times10^{-6}$
C_6	$(5.030\pm3.2)\times10^{-5}$	$(0.314\pm1.9)\times10^{-5}$	$(2.133\pm1.4)\times10^{-5}$	$(1.402\pm1.3)\times10^{-6}$
C_7	$(-0.199\pm1.5)\times10^{-5}$	$(2.227\pm5.7)\times10^{-6}$	$(-5.181\pm3.9)\times10^{-6}$	$(1.156\pm9.5)\times10^{-7}$
M_p	6.30±0.10	2.98±0.11	24.5±1.9	48.8±2.5
R_{ch}	4.31±0.03	4.03±0.04	5.08±0.11	4.89±0.04
χ^2/N	0.29	0.54	0.46	0.33

$2s_{1/2}$, $1d_{3/2}$) basis using an A-dependent residual interaction fitted to energy levels throughout the $A=17-39$ region.[3] We used oscillator wave functions with $b=1.835$ fm, corrected for the center-of-mass motion, to assemble $\rho^v(r)$.

The core contribution is based upon the Tassie shape[23]

$$C_\tau(r)\propto r^{J-1}\frac{d\rho_\tau^g}{dr}\ , \tag{10}$$

where ρ^g is the ground-state density. The normalizations are conveniently chosen so that

$$\int dr\, r^{J+2}C_\tau(r)=1\ . \tag{11}$$

In evaluating these densities, we have further assumed that $\rho_n^g=(N/Z)\rho_p^g$ and unfold the nucleon form factor from the charge density tabulated in Ref. 20.

The core contributions $\rho_\tau^c(r)=M_\tau^c C_\tau(r)$ are related to the valence densities by the polarization matrix δ defined by

$$M_p^c=\delta^{pp}M_p^v+\delta^{pn}M_n^v \tag{12a}$$

$$M_n^c=\delta^{np}M_p^v+\delta^{nn}M_n^v\ , \tag{12b}$$

where M_τ^v and M_τ^c are the valence and core contributions to the multipole moments M_τ. Brown *et al.*[3] assume that $\delta^{pp}=\delta^{nn}=\delta^{pn}=\delta^{np}=\delta_J$ and use $\delta_2=0.35$ and $\delta_4=0.50$. The matrix elements M_n and M_p that are predicted for the states of interest are listed in Table III and are separated into valence and core contributions.

IV. RESULTS

A. Proton transition densities

Electron scattering data for ^{30}Si are rather limited. Brain *et al.*[24] employed an enriched ^{30}Si target to obtain measurements for the two lowest 2^+ states for $0.4<q<1.1$ fm^{-1} relative to elastic scattering. We produced absolute form factors by calculating elastic scattering from the charge density of Ref. 20. Bernhardt[25] analyzed the ^{30}Si contaminants in spectra taken by Whitner *et al.*[26] with a natural ^{28}Si target and obtained data on the 2_1^+, 2_2^+, 3_1^-, and 4_2^+ states for $0.6<q<2.2$ fm^{-1}. These two experiments agree well where they overlap.

Fits to the form factor data are shown in Fig. 3. The

TABLE II. Neutron transition density parameters for ^{30}Si. LGE coefficients C_n are in units of fm^{-3} and are based upon $b=1.835$ fm. The units of M_n are fm^J and the units of R_n are fm.

	2_1^+	2_2^+	3_1^-	4_2^+
C_0	$(9.527\pm0.71)\times10^{-2}$	$(2.858\pm0.29)\times10^{-2}$	$(3.912\pm0.34)\times10^{-2}$	$(2.100\pm0.18)\times10^{-2}$
C_1	$(-4.719\pm0.39)\times10^{-2}$	$(-1.471\pm0.13)\times10^{-2}$	$(-2.294\pm0.16)\times10^{-2}$	$(-2.764\pm0.32)\times10^{-3}$
C_2	$(1.813\pm0.53)\times10^{-3}$	$(-1.522\pm0.23)\times10^{-3}$	$(1.722\pm0.33)\times10^{-3}$	$(-2.626\pm0.80)\times10^{-4}$
C_3	$(2.485\pm0.57)\times10^{-3}$	$(8.866\pm2.7)\times10^{-4}$	$(1.788\pm0.27)\times10^{-3}$	$(1.869\pm0.19)\times10^{-4}$
C_4	$(6.890\pm2.9)\times10^{-4}$	$(3.242\pm1.5)\times10^{-4}$	$(4.407\pm1.4)\times10^{-4}$	$(0.891\pm1.5)\times10^{-5}$
C_5	$(-2.053\pm1.9)\times10^{-4}$	$(-2.081\pm7.7)\times10^{-5}$	$(-2.508\pm0.99)\times10^{-4}$	$(-2.838\pm0.60)\times10^{-5}$
C_6	$(-1.838\pm1.3)\times10^{-4}$	$(-3.611\pm2.7)\times10^{-5}$	$(-1.368\pm0.65)\times10^{-4}$	$(4.076\pm3.8)\times10^{-6}$
C_7	$(-7.854\pm5.0)\times10^{-5}$	$(-7.780\pm4.6)\times10^{-6}$	$(-3.580\pm2.6)\times10^{-5}$	$(3.058\pm2.1)\times10^{-6}$
M_n	8.91±0.57	2.16±0.21	32.7±1.9	52.8±6.0
R_n	4.01±0.21	3.68±0.32	4.59±0.21	4.47±0.49
χ^2/N	6.5	9.6	6.1	2.4

TABLE III. Shell-model matrix elements for ^{30}Si in units of fm^J.

	2_1^+	2_2^+	4_1^+	4_2^+
M_p^V	3.52	2.62	25.79	32.02
M_p^C	2.77	0.91	33.36	17.70
M_p	6.29	3.53	59.15	49.72
M_n^V	4.40	-3.9×10^{-5}	40.94	3.37
M_n^C	2.77	0.91	33.36	17.69
M_n	7.17	0.91	74.31	21.06

data for the 2^+ states are sufficient to define two maxima in each form factor. The data for the 4_2^+ state exhibit only a single form factor peak as expected for a predominantly $d\rightarrow d$ transition. Fitted LGE coefficients and moments are listed in Table I.

Shell-model predictions for the positive-parity form factors are also shown in Fig. 3. We observe that the 2_1^+ and 2_2^+ form factors are fairly accurate for low momentum transfer, but that significant differences in the 2_2^+ form factor are observed for $q>1.4$ fm^{-1}. The calculated proton matrix elements M_p are also in good agreement with the data for these states. Finally, the shell model also provides an accurate form factor for the 4_2^+ state.

The data for the 3_1^- state, on the other hand, are somewhat more ambiguous and do not definitely exclude a second maximum beyond 2 fm^{-1}. However, we note that the fact that the 3^- data do not extend quite as far as the 2^+ data suggests that the form factor continues to fall and does not climb to a significant peak soon after 2 fm^{-1}. Although shell-model calculations are not available for negative-parity states of ^{30}Si, further guidance can be obtained by comparing form factors for the relevant single-particle transitions with the data. Several single-proton form factors, normalized to the peak of the fitted 3_1^- form factor, are compared with the data in Fig. 4. The $1p\rightarrow1d$ form factor is much broader than the data and, as expected, cannot represent a strong component of this transition. The $2s\rightarrow1f$ and $1d\rightarrow1f$ form factors are both similar to the data for low q, but the $2s\rightarrow1f$ form factor has a minimum at smaller momentum transfer and a much stronger second maximum than the $1d\rightarrow1f$ form factor. Although the data do not exclude a strong second maximum, they do indicate that a minimum, if present, is beyond 2.2 fm^{-1}. Furthermore, although the data fall somewhat faster than the $1d\rightarrow1f$ form factor, we note that a modest increase in radial scale could be obtained either from more realistic radial wave functions or from a surface-peaked core-polarization contribution. Either effect would improve the agreement between the data and the $1d_{5/2}\rightarrow1f_{7/2}$ form factor, which is expected to dominate. Therefore, we feel justified in suppressing the fitted form factor for $q>2.2$ fm^{-1}.

B. Neutron transition densities

Calculations of proton scattering based upon the predictions of the shell-model for positive-parity states are

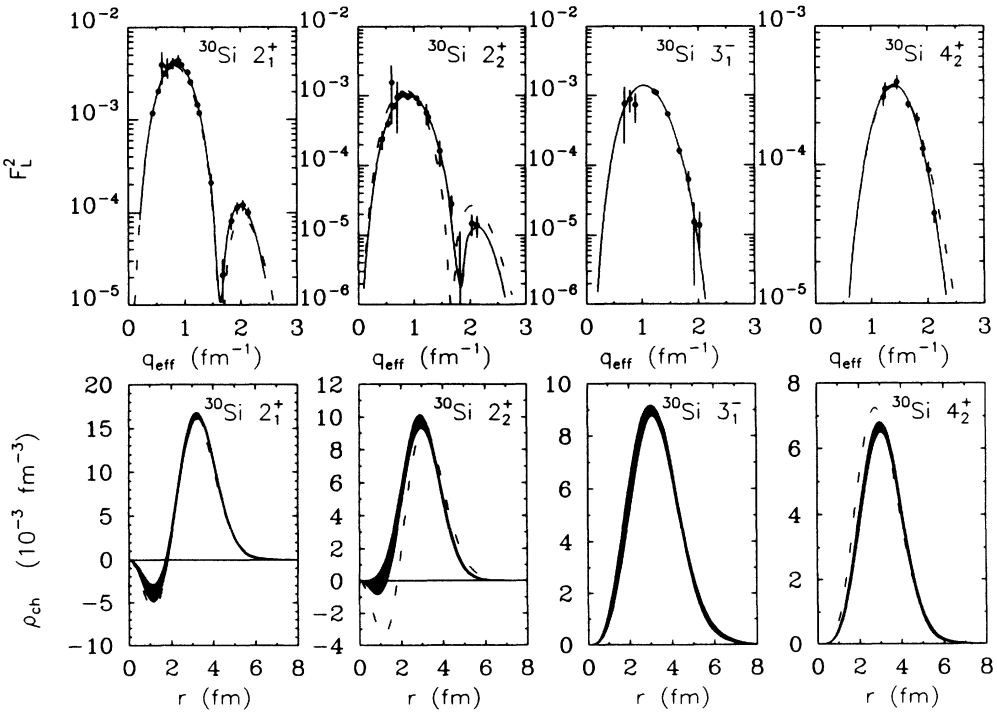

FIG. 3. Electron scattering data from Refs. 24 and 25 were fitted using the Laguerre-Gaussian expansion. The solid curves display fitted form factors and the dashed curves display the shell-model predictions of Brown, Radhi, and Wildenthal (Ref. 3). Fitted transition charge densities are shown with error bands that include truncation effects.

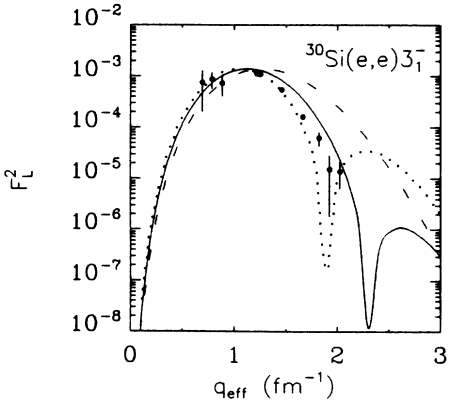

FIG. 4. Electron scattering data for the 3_1^- state of ^{30}Si are compared with normalized single-particle form factors for $1d_{5/2} \rightarrow 1f_{7/2}$ (solid), $2s_{1/2} \rightarrow 1f_{7/2}$ (dotted), and $1p_{1/2} \rightarrow 1d_{5/2}$ (dashed) transitions.

shown as dashed curves in Figs. 5 and 6. We find that the predicted cross sections are too small, especially for the 2_2^+ and 4_2^+ states. Recognizing that the shell-model predictions for the electromagnetic form factors were relatively accurate for low momentum transfers, the bulk of these discrepancies must be due to the predicted neutron densities. Similarly, the shell-model prediction for the 4_1^+ cross section is about a factor of 2 below the peak of the data. The analyzing power, which for normal-parity transitions is more sensitive to the interaction and the multipolarity than to details of structure, is described more accurately. However, in the absence of electron scattering data for the proton transition density, a fit of the neutron density is not possible for this state.

Fits to the 2_1^+, 2_2^+, 3_1^-, and 4_2^+ data using the LGE are shown as solid curves in Figs. 5–7. The fitted densities are shown in Fig. 8 as bands which include uncertainties due to penetrability, incompleteness, and normalization. To assess the sensitivity of the data to differences between the shapes of the neutron and proton transition densities, scale-factor fits to the data for $q < 1.5$ fm^{-1}, assuming $\rho_n = S\rho_p$, are shown as dotted curves. Both models fit the data quite well for low momentum transfers, but the higher-q data do show some sensitivity to shape differences. In particular, the 3_1^- cross section displays a prominent second maximum not present in the electromagnetic form factor or in the fit based upon scaling the proton density. However, because form factor data are unavailable for these momentum transfers, part of this difference may be due to inaccuracy in the proton transition densities. Nevertheless, the narrowness of the

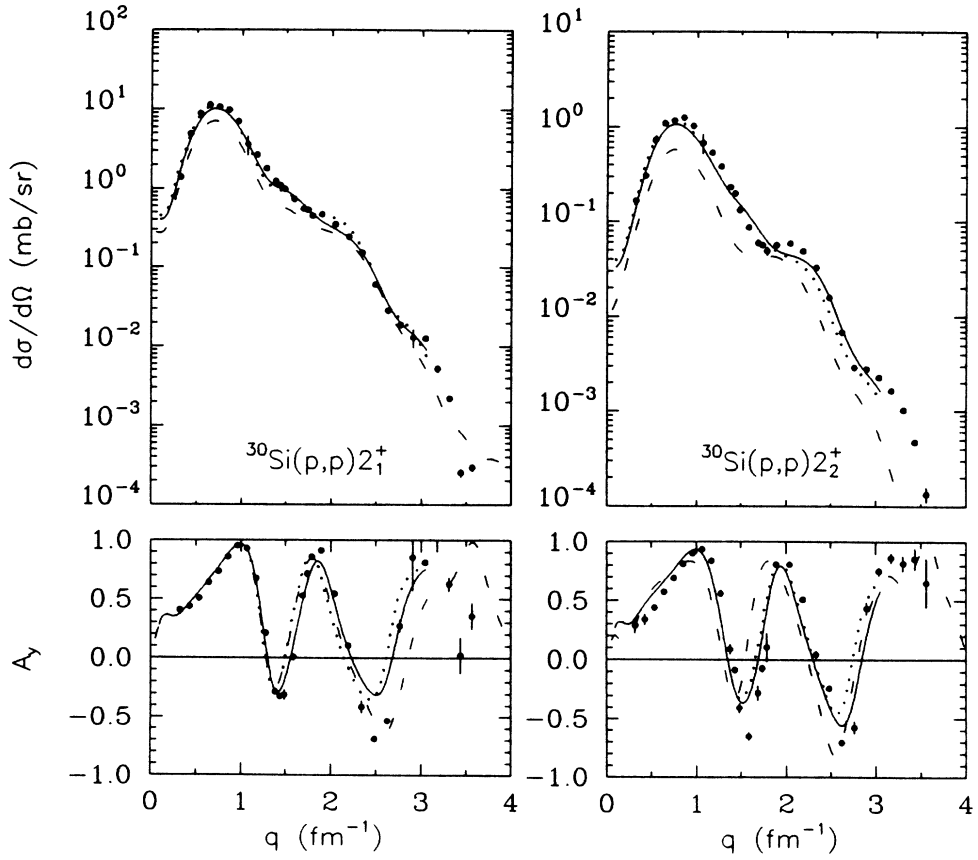

FIG. 5. Proton scattering data for the 2_1^+ and 2_2^+ states of ^{30}Si are compared with shell-model predictions (dashed), scale-factor fits to data with $q < 1.5$ fm^{-1} (dotted), and LGE fits to data with $q < 2.7$ fm^{-1} (solid). Data for larger q are displayed but were not included in the fits.

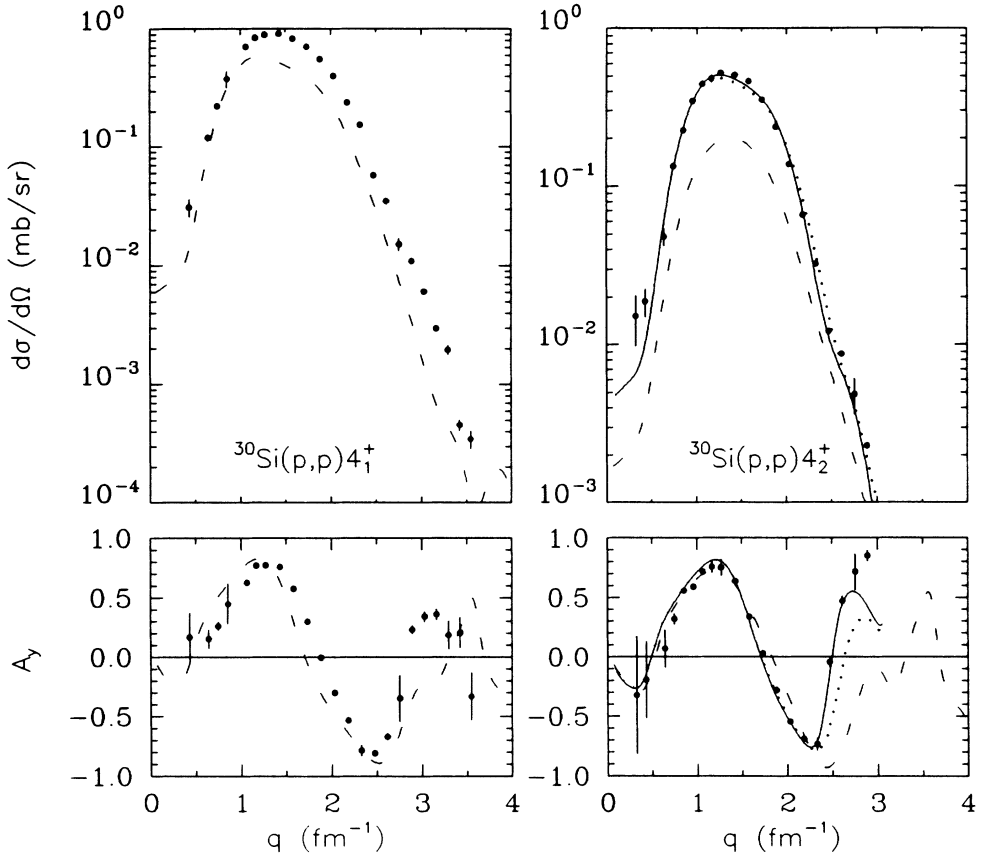

FIG. 6. Proton scattering data for the 4_1^+ and 4_2^+ states of ^{30}Si are compared with shell-model predictions (dashed), scale-factor fits to data with $q < 1.5$ fm^{-1} (dotted), and LGE fits to data with $q < 2.7$ fm^{-1} (solid). Data for larger q are displayed but were not included in the fits. Fits could not be performed for the 4_1^+ state because electron scattering data for the proton density are unavailable.

error bands on the fitted densities indicates the level of precision that would be possible should more complete (e,e') data become available.

The moments of the fitted densities are compared with the fitted scale factors in Table IV. The scale factors are systematically about 15% larger than the fitted M_n/M_p ratios. These factors were fitted to only the low-q data and produce slightly larger peak cross sections than do the more sophisticated LGE fits. However, despite the constraints placed upon the LGE analysis, the latter gives superior overall fits for $q < 2.7$ fm^{-1}. As there is little reason to expect the neutron and proton transition densities to be so similar in shape that scale factors would be more accurate than 15%, we favor the LGE results for M_n/M_p over the scale factors.

The M_n/M_p ratio for the 2_1^+ state that was deduced

TABLE IV. Ratios of M_n/M_p for ^{30}Si.

	Lifetime[a]	$(\pi^{\pm},\pi^{\pm})$[b]	(p,p')[c] S	(p,p')[c] LGE	Shell model[d]
2_1^+	1.22(6)	1.20(11)	1.55(10)	1.41(9)	1.14
2_2^+	0.52(3)		0.88(8)	0.72(7)	0.26
3_1^-			1.51(11)	1.33(13)	
4_1^+					1.26
4_2^+			1.16(10)	1.08(13)	0.42

[a]Reference 29.
[b]Reference 6.
[c]Present results.
[d]Reference 3.

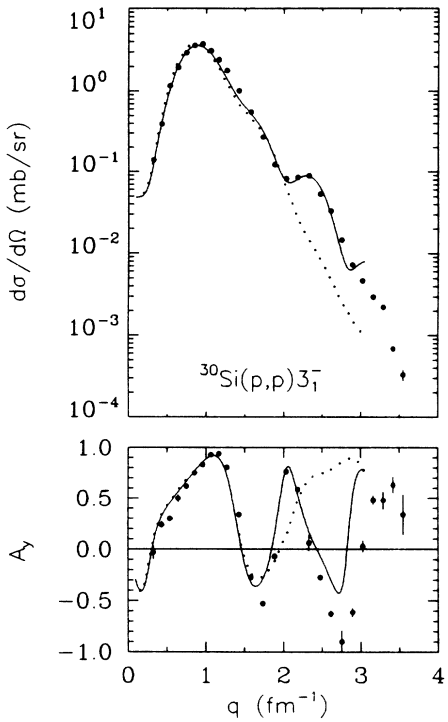

FIG. 7. Proton scattering data for the 3_1^- state of ^{30}Si were fitted assuming $\rho_n \propto \rho_p$ (dotted) or using the Laguerre-Gaussian expansion for ρ_n (solid). The pronounced cross section maximum near $q \sim 2.3$ fm^{-1} reveals the difference in shape between neutron and proton transition densities.

from data for the scattering of 162 MeV pions,[6] assuming $\rho_n \propto \rho_p$, is also listed in Table IV. Fortunately, the shapes of ρ_n and ρ_p for this state are sufficiently similar for this approach to be successful. However, Oakley and Fortune[27] have shown that plausible microscopic models for higher 2^+ states in several other nuclei fit 162 meV pion scattering data with M_n/M_p values very different from the results of the collective model. Hence, model dependence limits the applicability of pion scattering near the delta resonance to the simplest collective excitations. The present method for proton scattering data is more versatile. Additional data for 50 MeV pions[28] are omitted because that reaction gives M_n/M_p values systematically lower than the mirror method or 162 MeV pions.

Finally, Table IV also compares the fitted moments with matrix elements deduced from lifetime data for 2^+ states of the $A=30$ isotriplet by Alexander *et al.*[29] These values were deduced assuming charge independence and neglecting Coulomb and binding effects upon single-nucleon wave functions. However, Coulomb corrections to M_n/M_p are expected to be 10–20% for the lowest 2^+ state and larger corrections can be expected for higher states.[30] Therefore, we judge the agreement between electromagnetic and hadronic measurements of M_n/M_p for the 2^+ states of ^{30}Si to be acceptably within the realm of known variability.

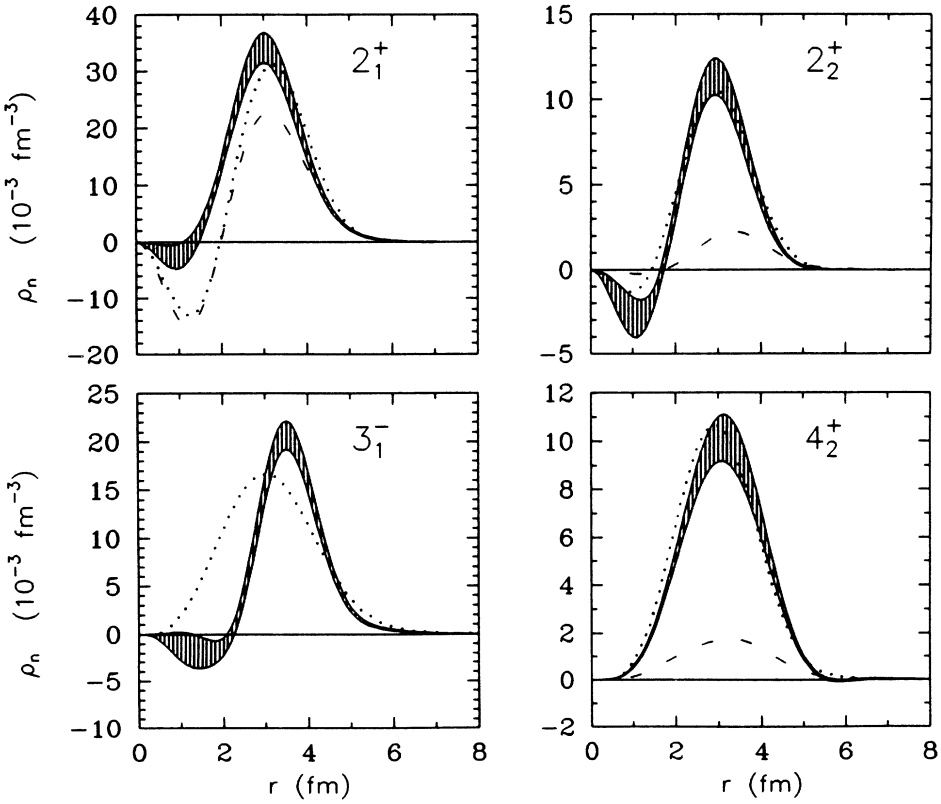

FIG. 8. Fitted neutron transition densities (bands) are compared with scale-factor fits (dotted lines) and shell-model predictions (dashed lines). Note that for positive-parity states the fitted neutron densities are similar in shape to the corresponding proton densities but are considerably stronger than shell-model predictions. For the 3_1^- state, the shape differences show that different orbitals participate for neutrons and protons.

C. Comparisons with the shell model

1. 2^+ states

Before shell-model calculations within a limited model space can be compared with experimental data, configurations outside the model space must be included in a correction for core polarization. The model of Brown, Radhi, and Wildenthal is based upon the assumption that core polarization can be described by a Tassie density normalized for each multipolarity to a common polarization parameter δ_J that is independent of state and mass. These parameters were obtained from a global analysis of electromagnetic data for the *sd*-shell based upon effective charges which, in our notation, take the form $e_p=1+\delta^{pp}$ and $e_n=\delta^{pn}$. Assuming that $\delta^{pp}=\delta^{pn}=\delta_J$, they found $\delta_2=0.35$ and $\delta_4=0.50$ provide good fits to the available $C2$ and $C4$ data.[31-34] Hence, it is not surprising that the shell model describes the present electron scattering data for ^{30}Si so well. Furthermore, we can infer that intruder configurations do not play especially important roles in these wave functions. However, the failure of the shell model to account for the neutron matrix elements suggests that the additional assumption $\delta^{nn}=\delta^{pp}=\delta^{np}=\delta^{pn}$ is too simplistic.

More generally, it is useful to define linear combinations

$$\delta^{p0}=\delta^{pp}+\delta^{pn},\quad \delta^{n0}=\delta^{nn}+\delta^{np}\ , \tag{13a}$$

$$\delta^{p1}=\delta^{pp}-\delta^{pn},\quad \delta^{n1}=\delta^{nn}-\delta^{np}\ , \tag{13b}$$

which describe proton and neutron polarizations induced by isoscalar $M_0^v=M_n^v+M_p^v$ and isovector $M_1^v=M_n^v-M_p^v$ components of the valence wave function, whereby

$$M_p=[(1+\delta^{p0})M_0^v-(1+\delta^{p1})M_1^v]/2\ , \tag{14a}$$

$$M_n=[(1+\delta^{n0})M_0^v+(1+\delta^{n1})M_1^v]/2\ . \tag{14b}$$

If we assume that the core polarization mechanism is charge symmetric, then we would expect $\delta^{p0}=\delta^{n0}$ and $\delta^{p1}=\delta^{n1}$. If we further assume the mechanism is charge independent, then we would also expect $\delta^{p1}=\delta^{n1}=0$. Using shell-model predictions for the valence contributions, Brown *et al.*[33] attempted to extract δ^{p1} from M_p data for $C2$ transitions throughout the *sd*-shell assuming again independence from state and mass. However, the dominance of M_0^v for most of the available data makes this task difficult. Furthermore, the isovector moment is rather sensitive to ambiguities in the single-particle wave functions and to Coulomb corrections. Using oscillator wave functions they found $\delta^{p1}\approx 0.0$, but other models yield values as large as $\delta^{p1}=-0.65$. Using local Woods-Saxon potentials and a quadrupole-quadrupole model of core polarization, their preferred result is $\delta^{p1}=-0.32$. Hence, charge independence of core polarization strengths is not well founded.

Furthermore, even the assumption of charge symmetry may be seriously flawed. Schematic model calculations made by Brown and Madsen[35-37] show that isospin impurities in the giant quadrupole resonances can produce large differences between δ^{pn} and δ^{np}. For example, they calculate $\delta^{pp}=0.31$, $\delta^{nn}=0.40$, $\delta^{np}=0.85$, and $\delta^{pn}=0.12$ for ^{207}Pb and similar values for ^{118}Sn.[35] More generally, the schematic model predicts $\delta^{nn}>\delta^{pp}$ and $\delta^{np}>\delta^{pn}$. Hence, although the model has not been applied to the *sd* shell, these results cast doubt upon the assumption of charge symmetry for core polarization.

If we assume that the shell model accurately predicts valence matrix elements for the lowest two 2^+ states of ^{30}Si, we can deduce all four polarization parameters from the four measured matrix elements. Because $M_n^v\approx 0$ for the 2_2^+ state, δ^{pp} and δ^{np} are determined by M_p and M_n, respectively. The resulting polarization matrix

$$\begin{bmatrix}\delta^{pp} & \delta^{pn}\\ \delta^{np} & \delta^{nn}\end{bmatrix}=\begin{bmatrix}0.14 & 0.52\\ 0.82 & 0.37\end{bmatrix} \tag{15}$$

satisfies the inequalities of the schematic model, but with a rather large ratio between δ^{nn} and δ^{pp}. Nevertheless, the proton polarization $\delta^{p0}=0.66$ for predominantly isoscalar transitions agrees well with the systematics of electron scattering in the *sd* shell ($\delta^{p0}=0.70$). However, the corresponding neutron polarization, $\delta^{n0}=1.19$, required to fit proton scattering data is almost twice as large.

A similar analysis of (e,e') and (p,p') data was made by Alons *et al.*[38] for ^{26}Mg, using coupled-channels fits to data for 24 MeV protons. A least-squares fit to the $C2$ matrix elements, including the $4^+\leftrightarrow 2^+$ and $2_1^+\leftrightarrow 2_2^+$ branches, was made using Chung-Wildenthal wave functions[32,39] for the valence space. The resulting polarization parameters for ^{26}Mg, $\delta^{pp}=0.16(2)$, $\delta^{nn}=0.61(19)$, $\delta^{np}=0.7(6)$, $\delta^{pn}=0.16(2)$, are in good agreement with our results for ^{30}Si. In particular, they also find δ^{nn} considerably larger than δ^{pp}. Presumably our results are more accurate because the reaction mechanism is simpler at 180 MeV than at 24 MeV.

It is also instructive to compare our results with the mass-dependent fit made by Alexander, Castel, and Towner[40] to M_p data in the *sd* shell using Brown, Radhi, and Wildenthal valence wave functions. Assuming charge symmetry, they find

$$\delta^{pp}=0.188+0.0035n\ , \tag{16a}$$

$$\delta^{pn}=0.317+0.012n\ , \tag{16b}$$

where n denotes the number of valence nucleons and where $\partial\delta^{pn}/\partial n$ was linked to $\partial\delta^{pp}/\partial n$ by a schematic model. Thus, this model also gives neutrons about twice the core polarization as protons. For ^{30}Si, in particular, this model predicts $\delta^{pp}=0.237$ and $\delta^{pn}=0.485$, which are roughly consistent with our results.

Finally, we note that Sagawa and Brown[41] have used an RPA calculation based upon a Skyrme interaction and Hartree-Fock wave functions to compute state-dependent isoscalar and isovector effective charges for $C2$ transitions in nuclei near either ^{16}O or ^{40}Ca. Although the resulting state dependence is relatively small, the mass dependence is pronounced and is consistent with the model of Alexander *et al.* Averaging these effective charges over state and mass should then produce results comparable to the global fits reported in Refs. 31–34 and to the charges appropriate to silicon, which lies near the

middle of the *sd* shell. This average isoscalar polarization, $\delta^{p0}=0.68$, agrees well with the global fit, $\delta^{p0}=0.72$, for ^{30}Si from Alexander *et al.* The average isovector polarization, $\delta^{p1}=-0.22$, also agrees well with the result, $\delta^{p1}=-0.25$, from Alexander *et al.*, but is somewhat smaller than our result, $\delta^{p1}=-0.38$. It is also within the range allowed by the global fits performed by Brown *et al.*[33] and is near their preferred value of $\delta^{p1}=-0.32$. Therefore, Sagawa and Brown predict substantially larger neutron polarization charge, $e_n=(\delta^{p0}-\delta^{p1})/2=0.46$, than proton polarization charge, $\delta e_p=(\delta^{p0}+\delta^{p1})/2=0.24$, in agreement with our findings. However, contrary to our findings their calculation would predict $\delta^{nn}\approx\delta^{pp}$ and $\delta^{np}\approx\delta^{pp}$ because their giant resonances retain isospin purity.

Does the core polarization mechanism really violate charge symmetry as strongly as our results suggest? In the absence of a good microscopic calculation of this effect in the *sd* shell, we must content ourselves with a few qualitative observations. First, the empirical effective interaction was fitted to ^{16}O data using charge symmetry to equate neutron and proton transition densities. Although effective charges for $2p2h$ and $4p4h$ excitations of the ^{16}O need not mimic those for $0\hbar\omega$ valence states, no evidence for significant violations of charge symmetry or for state dependence of the effective interaction has been seen.[9,22] Second, this same interaction provides a good description of proton scattering data for ^{28}Si.[10] Given that $M_n^v/M_p^v=1$ for self-conjugate nuclei, if δ^{n0}/δ^{p0} were really as large as 1.80 we would expect $M_n/M_p=1.32$ for ^{28}Si. The data are clearly not compatible with a violation of charge symmetry that is this large. Third, we have also found that fits of the empirical effective interaction made to data for ^{16}O and ^{40}Ca at several energies also give results independent of target and state and consistent with charge symmetry.[42] Fourth, fits of ρ_n made to $^{32}S(p,p')$ data at 318 MeV also satisfy charge symmetry at the 10% level.[43] Fifth, most calculations made with the schematic model that permit differences between δ^{n0} and δ^{p0} have been made for heavy nuclei with large Coulomb energies and different shells for valence neutrons and protons. It is not clear how applicable these results are to the *sd*-shell. Finally, we do not know the accuracy of the valence moments predicted by the shell model. In particular, delicate cancellations make M_n^v anomalously small for the 2_2^+ state of ^{30}Si. As a result, we find a rather large value for δ^{np} which may adversely affect some of the other parameters.

Thus, although it is clear that the neutron polarization charge is substantially larger than the proton polarization charge, it is not yet clear whether violations of charge symmetry are substantial. Therefore, the average isoscalar and isovector polarizations

$$\delta e_0=(\delta^{p0}+\delta^{n0})/2=0.92\ , \tag{17a}$$

$$\delta e_1=(\delta^{p1}+\delta^{n1})/2=-0.42\ , \tag{17b}$$

are probably more reliable than the individual values. These values imply effective charges $\delta e_p=0.25$ and $\delta e_n=0.67$ for $C2$ transitions that are consistent with the analysis of M_p data in the *sd* shell made by Alexander *et al.*[40] and with the calculations of Sagawa and Brown.[41] Further progress awaits more systematic experimental surveys of neutron transition densities and more sophisticated theoretical treatments of core polarization in the *sd* shell.

2. 4^+ states

The discrepancies between shell-model calculations assuming $\delta^{pp}=\delta^{pn}=0.5$ and proton scattering data for the 4^+ states are even larger than for the 2^+ states, even though the predicted 4_2^+ charge form factor is relatively accurate. However, in the absence of electron scattering data for the 4_1^+ state, it is not possible to deduce the full $C4$ polarization matrix. Therefore, we assume $\delta^{nn}=\delta^{pp}$ and $\delta^{np}=\delta^{pn}$ and deduce polarizations $\delta^{pp}=0.37$ and $\delta^{pn}=1.51$ that reproduce the experimental M_n and M_p data for the 4_2^+ state. Combining these polarizations with valence matrix elements calculated for the 4_1^+ state enhances M_n+M_p by a factor of 1.44 over the Brown, Radhi, and Wildenthal prediction. Consequently, the cross section is increased by about a factor of 2 and the agreement with the proton scattering data for the 4_1^+ state is much improved. Therefore, the data suggest that the neutron polarization charge $\delta e_n=1.51$ is much larger than the proton polarization charge $\delta e_p=0.37$ and that this enhancement is stronger for $C4$ than for $C2$ transitions.

These results can be compared with the Sagawa and Brown calculation for $C4$ excitations,[44] which predicts $\delta e_p=0.30$ and $\delta e_n=0.60$. The resulting isoscalar polarization $\delta e_0=0.90$ was shown to give accurate form factors for 4^+ excitations of the self-conjugate nuclei ^{24}Mg and ^{28}Si. However, our results suggest an isoscalar polarization $\delta e_0=1.88$ that is twice as large and not consistent with electron scattering data for nearby nuclei in the *sd* shell. The rather large value we obtain for δ^{pn} can again be traced to the small value of M_n^v for the 4_2^+ state. This observation suggests that the 4_2^+ valence wave function may not be sufficiently accurate to permit extraction of core polarization coefficients. However, we note that the strength of the 4_1^+ cross section also cannot be explained without substantial enhancements of either δe_0 or M_0^v. Although the 3_2^+ state could not be resolved from the 4_1^+ peak, the analyzing power data show no sign of contamination. Hence, we believe the 3_2^+ contribution is negligible. Finally, we note that strong multistep excitation of the 4^+ states is unlikely because both 4^+ analyzing powers retain the strong oscillatory pattern characteristic of direct excitation of normal-parity states. Therefore, although δ^{pn} probably is substantially larger than δ^{pp} for $C4$ transitions, we conclude that the available wave functions are not sufficiently accurate to permit extraction of these quantities from the data for ^{30}Si.

Alternatively, part of the enhancement of M_n for the 4_2^+ state may be due to an explicit $f_{7/2}^2$ neutron-pair admixture into the ^{30}Si ground-state wave function. In Fig. 9 the form factor obtained by recoupling an $f_{7/2}^2$ pair to 4^+ is compared with 4_2^+ form factor predicted by the *sd* shell model and with the neutron form factor fitted to the

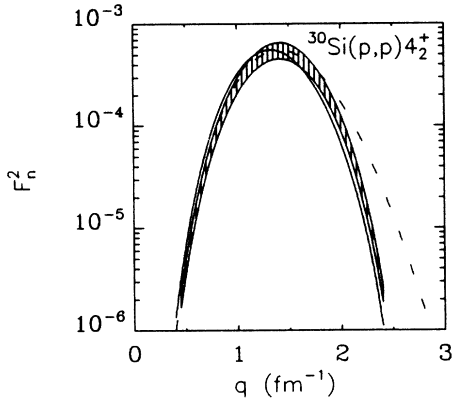

FIG. 9. The neutron form factor (band) fitted to ^{30}Si($\vec{p},p'$) data for the 4_2^+ state is compared with an $f_{7/2}^2$ form factor (solid) and the shell-model charge form factor (dashed). The solid and dashed curves are both normalized to the peak of the fitted F_n^2.

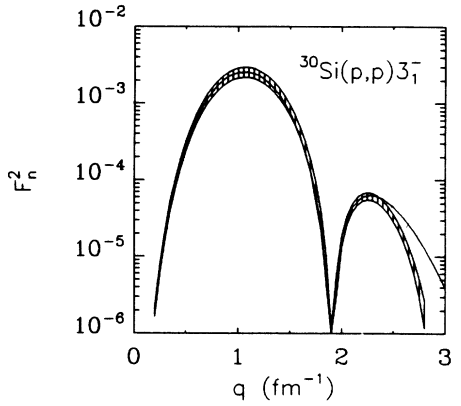

FIG. 10. The neutron form factor (band) fitted to ^{30}Si($\vec{p},p'$) data for the 3_1^- state is compared with a $2s_{1/2}\rightarrow 1f_{7/2}$ single particle form factor (solid) normalized at the first peak.

4_2^+ proton scattering data. Although these three form factors are all similar for $q<2$ fm^{-1}, the data appear to favor the $f_{7/2}^2$ shape. We also note that an $f_{7/2}^2$ neutron-pair 6^+ state has been observed at 8.93 MeV in the reaction ^{28}Si(α,^{2}He)^{30}Si at $E_\alpha=65$ MeV, a transfer reaction which preferentially populates stretched neutron-pair configurations.[45,46] Based upon the spacing of $f_{7/2}^2$ states in ^{42}Ca (Ref. 47), we can expect a 4^+ state of similar structure to occur approximately 0.4 MeV lower, near 8.5 MeV. Although we do not know whether this energy is low enough for the $f_{7/2}^2$ configuration to mix significantly with the *sd* shell configurations, the present data suggest that this possibility is worth exploring with an extended-basis shell-model calculation.

3. 3_1^- state

The dotted curve shown in Fig. 7 for the 3_1^- state was obtained by scaling a neutron density with the same shape as the proton density fitted to (e,e') data assuming dominance of the $1d_{5/2}\rightarrow 1f_{7/2}$ configuration. The latter form factor possesses only a single maximum. Consequently, the scale factor analysis fails to reproduce the pronounced maximum in the (p,p') cross section near 2.3 fm^{-1}.

In addition to the $1d_{5/2}\rightarrow 1f_{7/2}$ contribution, the neutron transition density is expected to include a substantial $2s_{1/2}\rightarrow 1f_{7/2}$ component. Note that the $(1f_{7/2}2s_{1/2})_{3^-}$ neutron configuration dominates the single-neutron transfer reaction ^{29}Si(d,p)^{30}Si for the 3_1^- state.[48,49] In Fig. 10, we compare the fitted neutron form factor $F_n^2(q)$ with a renormalized $2s_{1/2}\rightarrow 1f_{7/2}$ form factor. The agreement between these shapes is truly remarkable and shows that this configuration is indeed an important component of the 3_1^- wave function. The $2s\rightarrow 1f$ contribution is revealed clearly by the second maximum of F_n^2 and is required to fit the proton scattering data. The resulting difference between the shapes of the neutron and proton transition densities, shown in Fig. 8, is much greater for the 3_1^- state than for the positive-parity states. Therefore, by fitting radial densities we have obtained a considerably more detailed picture of the microscopic structure of the transition than could have been obtained from conventional scale-factor analyses.

Actually, the agreement is perhaps a little too good given that the $d\rightarrow f$ configuration should make a significant contribution to the first peak of the form factor but not to the second. Hence, we should expect the ratio between these peaks to be somewhat larger for a mixed transition than for the pure $2s\rightarrow 1f$ transition. A small admixture of $2s\rightarrow 1f$ can be introduced into the proton form factor without spoiling the fit to the available electron scattering data. This admixture would enhance the proton form factor for $q>2$ fm^{-1} and reduce the corresponding neutron form factor. More extensive electron scattering data are needed to confirm this hypothesis.

D. Reaction mechanism uncertainties

Miskimen *et al.*[17] have studied the effect of coupling between the 2_1^+ and 2_2^+ states on the cross sections calculated for protons with energies between 200 and 800 MeV. Using shell-model matrix elements, they found that effects of ± 7–8 %, depending on the assumed signs, could be expected at the peak of the angular distribution. The effect on the angular distribution appeared almost uniform. However, the results they obtained at 650 MeV for the second 2^+ were in rather poor agreement with the data presumably because the model densities do not describe these states with sufficient accuracy. Also, the impulse approximation is poor for 500–650 MeV proton scattering. Furthermore, we might expect the effect of channel coupling to be reduced when more states with random phases are included. Finally, we note that multistep contributions would probably have a substantial effect upon analyzing powers, whereas the present direct calculations are quite accurate for analyzing powers

whether or not A_y data are included in the fits.

Nevertheless, these results can be used to estimate the maximum errors that might be incurred by neglect of multistep contributions. The systematic uncertainty of 10% we have applied to the cross section normalization is larger than the likely effect of channel coupling. Hence, we believe that the estimated error bands are large enough to encompass uncertainties in the reaction mechanism.

Other uncertainties include residual errors in the effective interaction. Most notably, in the absence of data for calibration of the density dependence of the isovector components, we use the G-matrix calculation of von Geramb *et al.*[19] for these contributions. Fortunately, isoscalar components of both the effective interaction and the nuclear structure are generally much stronger than the corresponding isovector components so that residual errors in isovector parts of the interaction should have little impact upon the states considered herein. We find that neglecting the density dependence of the isovector interaction produces changes in the fitted densities that lie within the present error envelopes.

The best method of testing the accuracy of fitted neutron transition densities, independent of unreliable structure calculations, is to repeat the analysis using proton scattering data taken at another energy for which an accurate empirical effective interaction is also available. If the two energies are sufficiently different, then their residual errors should be uncorrelated and the difference between the two fitted densities should be a reliable and practical guide to the accuracy of the reaction mechanism. This test is presently being applied for both ^{48}Ca and ^{88}Sr.[42,50]

V. SUMMARY AND CONCLUSIONS

We have obtained cross section and analyzing power measurements for several states of ^{30}Si using 180 MeV protons. Proton densities were fitted to existing electron scattering data. Neutron densities were fitted to the proton scattering data using an empirical density-dependent effective interaction previously fitted to 180 MeV proton scattering data for ^{16}O and ^{28}Si. The moments we deduced for the two 2^+ neutron densities agree well with matrix elements deduced from pion scattering and with lifetime data for the $A=30$ nuclei with $T=1$. This result supports the accuracy of our analysis.

We have found that the shell model provides a good description of the proton densities for the positive-parity states, but that its predictions for the neutron contributions are generally too small. Specifically, the shell model predicts matrix-element ratios $M_n/M_p=1.14$, 0.26, and 0.42 for the 2_1^+, 2_2^+, and 4_2^+ states, whereas we find values of 1.41(9), 0.72(7), and 1.08(13). Hence, the discrepancies are modest for the lowest 2^+ state but are particularly large for the second 2^+ and 4^+ states. If the valence wave functions are accurate, the data require the neutron effective charge δ^{pn} to be substantially larger than the proton effective charge δ^{pp}. However, more detailed structure calculations are required to resolve some of the remaining inconsistencies.

Although, shape differences between fitted neutron and proton densities are modest for the positive-parity states, the differences between neutron and proton form factors fitted to the 3_1^- data are quite revealing. We find that the 3_1^- proton form factor is dominated by the $1d_{5/2}\rightarrow 1f_{7/2}$ transition, whereas the neutron form factor exhibits a clear $2s_{1/2}\rightarrow 1f_{7/2}$ signature. Also, we find $M_n/M_p=1.33(13)$ for this state.

By analyzing both electron and proton scattering data in a consistent manner, it is possible to obtain both proton and neutron transition densities. For simple surface-peaked densities, the deduced matrix elements agree well with the results obtained from lifetime measurements, pion scattering, or scale-factor fits of proton scattering. However, our methods are applicable to a much larger class of transitions than can be studied by lifetime measurements and are capable of providing considerably more detailed and more accurate data on neutron transition densities than can be obtained from pion scattering. This information should provide critical new tests of nuclear structure theories. Therefore, a versatile new technique is available for studying nuclear structure and we are applying these methods vigorously. We hope that interest in nuclear structure will be renewed by the detailed measurements of neutron transition densities now becoming available.

ACKNOWLEDGMENTS

We would like to thank Dr. D. J. Millener, Dr. V. R. Brown, and Dr. B. H. Wildenthal for helpful discussions. This work was supported in part by grants from the National Science Foundation.

[1] J. Heisenberg, Adv. Nucl. Phys. **12**, 61 (1981).
[2] J. Heisenberg and H. P. Blok, Annu. Rev. Nucl. Part. Sci. **33**, 569 (1983).
[3] B. A. Brown, R. Radhi, and B. H. Wildenthal, Phys. Rep. **101**, 313 (1983).
[4] A. M. Bernstein, V. R. Brown, and V. A. Madsen, Phys. Rev. Lett. **42**, 425 (1979).
[5] A. M. Bernstein, V. R. Brown, and V. A. Madsen, Phys. Lett. **103B**, 255 (1981).
[6] C. L. Morris, S. J. Seestrom-Morris, D. Dehnhard, C. L. Blilie, R. Gilman, G. P. Gilfoyle, J. D. Zumbro, M. G. Burlein, S. Mordechai, H. T. Fortune, L. C. Bland, M. Brown, D. P. Saunders, P. A. Seidl, C. F. Moore, K. Maeda, G. S. Blanpied, and B. A. Brown, Phys. Rev. C **35**, 1388 (1987).
[7] J. J. Kelly, Phys. Rev. C **37**, 520 (1988).
[8] J. Kelly, W. Bertozzi, T. N. Buti, J. M. Finn, F. W. Hersman, M. V. Hynes, C. Hyde-Wright, B. E. Norum, A. D. Bacher, G. T. Emery, C. C. Foster, W. P. Jones, D. W. Miller, B. L. Berman, J. A. Carr, and F. Petrovich, Phys. Lett. **169B**, 157 (1986).
[9] J. J. Kelly, J. M. Finn, W. Bertozzi, T. N. Buti, F. W. Hersman, C. Hyde-Wright, M. V. Hynes, M. A. Kovash, B. Mur-

dock, P. Ulmer, A. D. Bacher, G. T. Emery, C. C. Foster, W. P. Jones, D. W. Miller, and B. L. Berman, (paper I) Phys. Rev. C **41**, 2504 (1990).

[10]Q. Chen, J. J. Kelly, P. P. Singh, M. C. Radhakrishna, W. P. Jones, and H. Nann, (paper II) Phys. Rev. C **41**, 2514 (1990).

[11]Q. Chen, Ph.D. thesis, Indiana University, 1988.

[12]P. Schwandt, H. O. Meyer, W. W. Jacobs, A. D. Bacher, S. E. Vigdor, M. D. Kaitchuck, and T. R. Donoghue, Phys. Rev. C **26**, 55 (1982).

[13]See AIP document no. PAPS PRVCA-41-2525-8 for 8 pages containing a complete tabulation of the data described in this paper. Order by PAPS number and journal reference from American Institute of Physics, Physics Auxiliary Publication Service, 335 E. 45th Street, New York, NY 10017. The price is $1.50 for each microfiche or $5.00 for photocopies. Air mail additional. Make checks payable to the American Institute of Physics.

[14]F. Petrovich, R. J. Philpott, A. W. Carpenter, and J. A. Carr, Nucl. Phys. **A425**, 609 (1984).

[15]B. Dreher, J. Friedrich, K. Merle, H. Rothaas, and G. Lührs, Nucl. Phys. **A235**, 219 (1974).

[16]H. G. Andresen, H. Peter, M. Müller, and H. J. Ohlbach, computer program HADES (unpublished).

[17]R. A. Miskimen, A. M. Bernstein, G. Bernhardt, C. F. Williamson, B. A. Brown, and R. Alarcon, Phys. Rev. C **37**, 1600 (1988).

[18]J. J. Kelly, computer program LEA (unpublished).

[19]H. V. von Geramb, in *The Interaction Between Medium Energy Nucleons in Nuclei—1982,* AIP Conf. Proc. No. 97, edited by Hans-Otto Meyer (AIP, New York, 1982), p. 44; L. Rikus, K. Nakano, and H. V. von Geramb, Nucl. Phys. **A414**, 413 (1984).

[20]H. de Vries, C. W. de Jager, and C. de Vries, At. Data Nucl. Data Tables **36**, 495 (1987).

[21]T. Cheon, K. Takayanagi, and K. Yazaki, Nucl. Phys. **A437**, 301 (1985); **A445**, 227 (1985); T. Cheon and K. Takayanagi, Nucl. Phys. **A455**, 653 (1986).

[22]J. J. Kelly, Phys. Rev. C **39**, 2120 (1989).

[23]L. J. Tassie, Austr. J. Phys. **9**, 407 (1956).

[24]S. W. Brain, A. Johnston, W. A. Gillespie, E. W. Lees, and R. P. Singhal, J. Phys. G **3**, 821 (1977).

[25]G. Bernhardt, M. S. thesis, MIT, 1983.

[26]K. E. Whitner, C. F. Williamson, B. E. Norum, and S. Kowalski, Phys. Rev. **22**, 374 (1980).

[27]D. S. Oakley and H. T. Fortune, Phys. Rev. C **37**, 1126 (1988).

[28]U. Wienands, N. Hessey, B. M. Barnett, F. M. Rozon, H. W. Roser, A. Altman, R. R. Johnson, D. R. Gill, G. R. Smith, C. A. Wiedner, D. M. Manley, B. L. Berman, H. J. Crawford, and N. Grion, Phys. Rev. C **35**, 708 (1987).

[29]T. K. Alexander, G. C. Ball, J. S. Forster, W. G. Davies, I. V. Mitchell, and H. B. Mak, Phys. Rev. Lett. **49**, 438 (1982).

[30]B. A. Brown, A. Arima, and J. B. McGrory, Nucl. Phys. **A277**, 77 (1977).

[31]B. H. Wildenthal, Nukleonika **23**, 459 (1978).

[32]B. A. Brown, W. Chung, and B. H. Wildenthal, Phys. Rev. C **22**, 774 (1980).

[33]B. A. Brown, B. H. Wildenthal, W. Chung, S. E. Massen, M. Bernas, A. M. Bernstein, R. Miskimen, V. R. Brown, and V. A. Madsen, Phys. Rev. C **26**, 2247 (1982).

[34]B. A. Brown, W. Chung, and B. H. Wildenthal, Phys. Rev. C **21**, 2600 (1980).

[35]V. R. Brown and V. A Madsen, Phys. Rev. C **11**, 1298 (1975).

[36]V. R. Brown and V. A. Madsen, Phys. Rev. C **17**, 1943 (1978).

[37]V. A. Madsen and V. R. Brown, Phys. Rev. Lett. **52**, 176 (1984).

[38]P. W. F. Alons, H. P. Blok, J. F. A. van Hienen, and J. Blok, Nucl. Phys. **A367**, 41 (1981).

[39]W. Chung, Ph.D. thesis, Michigan State University, 1978.

[40]T. K. Alexander, B. Castel, and I. S. Towner, Nucl. Phys. **A445**, 189 (1985).

[41]H. Sagawa and B. A. Brown, Nucl. Phys. **A430**, 84 (1984).

[42]J. J. Kelly, Bull. Am. Phys. Soc. **32**, 1120 (1987); A. E. Feldman, P. Boberg, B. S. Flanders, S. D. Hyman, J. J. Kelly, M. A. Khandaker, H. Seifert, P. Karen, B. E. Norum, A. Saha, and S. Nanda, *ibid.* **33**, 1570 (1988); H. Seifert, A. E. Feldman, B. S. Flanders, J. J. Kelly, M. Khandaker, Q. Chen, P. Karen, B. E. Norum, P. Welch, and A. Scott, *ibid.* **33**, 1570 (1988).

[43]M. A. Khandaker, A. E. Feldman, B. S. Flanders, J. J. Kelly, H. Seifert, P. Karen, B. E. Norum, and P. Welch, Bull. Am. Phys. Soc. **34**, 1233 (1989).

[44]H. Sagawa and B. A. Brown, Phys. Lett. **150B**, 247 (1985).

[45]R. J. de Meijer, R. Kamermans, J. van Driel, and H. P. Morsch, Phys. Rev. C **16**, 2442 (1977).

[46]R. Jahn, D. P. Stehl, G. J. Wozniak, R. J. de Meijer, and J. Cerny, Phys. Rev. C **18**, 9 (1978).

[47]P. M. Endt and C. van der Leun, Nucl. Phys. **A310**, 1 (1978).

[48]H. Mackh, H. Oeschler, G. J. Wagner, D. Dehnhard, and H. Ohnuma, Nucl. Phys. **A202**, 497 (1973).

[49]A. M. Baxter and S. Hinds, Nucl. Phys. **A211**, 7 (1973).

[50]B. S. Flanders, J. J. Kelly, K. K. Seth, B. Parker, M. Artuso, R. Soundranayagm, F. W. Hersman, and J. P. Connelly, Bull. Am. Phys. Soc. **32**, 1121 (1987).